ACI MATERIALS JOURNAL TECHNICAL PAPER

Title no. 107-M48

# Planar Image-Based Reconstruction of Pervious Concrete Pore Structure and Permeability Prediction

by Milani S. Sumanasooriya, Dale P. Bentz, and Narayanan Neithalath

*Transport properties of porous materials such as pervious concretes are inherently dependent on a variety of pore structure features. Empirical equations are typically used to relate the pore structure of a porous material to its permeability. In this study, a computational procedure is employed to predict the permeability of 12 different pervious concrete mixtures from three-dimensional (3D) material structures reconstructed from starting planar images of the original material. Two-point correlation (TPC) functions of the two-dimensional (2D) images from real pervious concrete specimens are employed along with the measured volumetric porosities in the reconstruction process. The pore structure features of the parent material and the reconstructed images are found to be similar. The permeabilities predicted using Darcy's law applied to the reconstructed structures and the experimentally measured permeabilities of pervious concretes are found to be in reasonably good agreement. The 3D reconstruction process provides a relatively inexpensive method (instead of methods such as X-ray tomography) to explore the nature of the pore space in pervious concretes and predict permeability, thus facilitating its use in understanding the changes in pore structure as a result of changes in mixture proportions.*

**Keywords:** permeability; pervious concrete; porosity; three-dimensional reconstruction.

## INTRODUCTION

The use of pervious concrete (enhanced porosity concrete) has been recognized by the Environmental Protection Agency (EPA) as one of the best management practices in reducing stormwater runoff, mainly due to its capability to permeate large quantities of water through its connected pore structure. The use of gap-graded aggregates, little or no fine aggregates, and low water-cement ratios (*w*/*c*) results in a material structure that consists of relatively large pores (2 to 8 mm [0.078 to 0.314 in.], compared to the micrometer-sized pores in conventional concretes) and a highly connected pore network.[1-3] The porosity of pervious concretes typically ranges from 15 to 30%.[1,4-8] Other environmental benefits of pervious concrete that are attributed to its unique pore structure include a reduction in the noise generated by tire-pavement interaction,[2,9] and a reduction in the urban heat island effect.[1,7]

Permeability, which is the most important functional property of pervious concrete, is typically related to the accessible porosity (connected porosity) in the material structure. The influence of mixture proportioning on the porosity and flow characteristics of pervious concretes have been experimentally investigated.[4,10] For porous materials, the water transport characteristics are also dependent on other pore structure features such as pore sizes, pore connectivity, and the specific surface area of the pores, as can be observed from a variety of pore structure-transport relationships such as the Kozeny-Carman[11] and Katz-Thompson[12] equations. It has been found from previous studies that the aforementioned pore structure features of pervious concretes vary significantly with changes in aggregate size and composition even when their porosities do not change appreciably.[4,8,9] The use of electrical impedance-based methods to extract the pore structure features that are significant in water transport and acoustic wave propagation through pervious concretes have been previously reported.[4,9] Computational material science-based approaches have been successfully used to study cement hydration and microstructure and property development in conventional cement-based materials.[13-16] Recent studies[17] have successfully used a virtual pervious concrete pore structure for permeability estimation. This study deals with three-dimensional (3D) reconstruction of pervious concrete material structures from two-dimensional (2D) images of real pervious concrete specimens and the use of these reconstructed structures to predict the permeability. The comparison between the pore structure features of the real and reconstructed pervious concretes are also carried out to evaluate the accuracy of the reconstruction process in retaining the pore structure features of the original material.

## RESEARCH SIGNIFICANCE

Pervious concrete has a random and complex pore structure (for example, pore volume, sizes, shapes, connectivity, and dispersion), many of the features of which are not easily determined experimentally from 2D images. Because volumetric porosity of such a macroporous material is obtained relatively easily and empirical property-porosity relationships are available, it has been customary to use porosity as the most distinguishing characteristic of pervious concretes. Many of the properties of such porous materials are also dependent on other pore structure features. In addition, for a random heterogeneous material such as pervious concrete, there will also be an inherent variability in the pore structure features. A better understanding of the influence of the pore structure parameters on the performance of pervious concretes is essential to develop materials science-based design procedures and better test methods for performance. Computational materials science-based tools are better equipped to deal with random porous media such as pervious concretes to achieve this objective. This study is an effort in that direction, where 3D pervious concrete structures reconstructed from starting 2D images of the real material are used to predict permeability. The reconstruction process facilitates the generation of any number of 3D images from planar sections without resorting to expensive 3D imaging techniques such as tomography. Being able to adequately

*ACI Materials Journal*, V. 107, No. 4, July-August 2010.
MS No. M-2009-341.R1 received October 15, 2009, and reviewed under Institute publication policies.  Pertinent discussion including authors' closure, if any, will be published in the May-June 2011 *ACI Materials Journal* if the discussion is received by February 1, 2011.

*ACI member* **Milani S. Sumanasooriya** *is a Graduate Student in the Department of Civil and Environmental Engineering at Clarkson University, Potsdam, NY. She received her bachelor's degree from University of Peradeniya, Peradeniya, Sri Lanka. Her research interests include the characterization and modeling of macroporous concretes.*

*ACI member* **Dale P. Bentz** *is a Chemical Engineer in the Materials and Construction Research Division, National Institute of Standards and Technology (NIST), Gaithersburg, MD. He is a member of ACI Committees 231, Properties of Concrete at Early Ages; 236, Material Science of Concrete; and 308, Curing Concrete. He received his BS in chemical engineering from the University of Maryland, College Park, MD, and his MS in computer and information science from Hood College, Frederick, MD. His research interests include experimental and computer modeling studies of the microstructure and performance of materials.*

*ACI member* **Narayanan Neithalath** *is an Associate Professor in the Department of Civil and Environmental Engineering at Clarkson University. He is Secretary of ACI Committee 522, Pervious Concrete, and a member of ACI Committees 123, Research and Current Developments; 232, Fly Ash and Natural Pozzolans in Concrete; and 236, Material Science of Concrete. He received his PhD from Purdue University, West Lafayette, IN. His research interests include characterization and performance evaluation of normal and enhanced porosity cementitious systems, sensing methods for in-place performance evaluation, and cement-free binder systems.*

predict the volume behavior of the material from planar images is a desirable feature for material design because it is generally straightforward to obtain such 2D information, especially at the millimeter resolution scale required for extracting the pores in pervious concrete.

## EXPERIMENTAL PROGRAM

### Materials and mixture proportions

In this study, 12 different pervious concrete mixtures were proportioned using three different single-sized coarse aggregates (pea gravel) and their blends. These mixtures are part of a larger study that was designed to evaluate the influence of material design parameters on the pore structure of pervious concretes. The aggregates were sieved into three different sizes: 1) No. 8 (2.36 mm [0.095 in.]) (passing through a No. 4 sieve (4.75 mm [0.19 in.]) and retained on a No. 8 sieve (2.36 mm [0.095 in.]), 2) No. 4 (4.75 mm [0.19 in.]) (passing through 9.5 mm [3/8 in.] and retained on a No. 4 sieve (4.75 mm [0.19 in.]), and 3) 9.5 mm (3/8 in.) (passing through a 12.5 mm [0.5 in.] sieve and retained on a 9.5 mm [3/8 in.] sieve). The pervious concrete mixtures were made using either one of these single-sized aggregates or a blend of any two single-sized aggregates by mass. The mixture identification provided in this paper gives the percentages of either the single-sized aggregates or the blends by mass. For instance, 75 – #8 – 25 – 3/8" refers to the mixture with 75% of the total aggregate by mass consisting of No. 8 aggregates and 25% of 3/8 in. (9.5 mm) aggregates. Type I ordinary portland cement was used as the binder. Fine aggregates were not used in any of the mixtures. For all the mixtures, the *w/c* by mass was kept constant at 0.33 and the aggregate-cement ratio by mass at 5. The cement content of all the mixtures was approximately 300 kg/m$^3$ (505 lb/yd$^3$). The mixtures were prepared in a laboratory mixer and cast in 100 mm (4 in.) diameter x 200 mm (8 in.) tall cylindrical molds.

For experimental determination of permeability, 95 mm (3.8 in.) diameter x 150 mm (6 in.) long specimens were used, which were obtained by placing 95 mm (3.8 in.) diameter x 200 mm (8 in.) long sleeves inside the 100 mm (4 in.) diameter molds during casting and then cutting the hardened specimen to the final length. The mixtures were compacted using a combination of vibration and tamping. All of the specimens were cured in a moist chamber (>98% relative humidity [RH]) for at least 7 days before they were subjected to pore structure characterization or permeability testing.

### Volumetric porosity and permeability determination

The effective volumetric porosities ($\phi_V$) of the pervious concrete mixtures were determined using a commonly adopted procedure where the mass of water required to fill a pervious concrete specimen enclosed in a latex sleeve is measured.[4,6,8] The hydraulic conductivities $K$ of the pervious concrete specimens were determined using a falling head permeameter, the details of which have been published extensively.[1,2,4,6]

The hydraulic conductivity $K$ was converted to intrinsic permeability $k$ using the density (1000 kg/m$^3$ [62.4 lb/yd$^3$]) and viscosity ($10^{-3}$ Pa·s [$145 \times 10^{-9}$ psi·s]) of water, and the acceleration due to gravity (9.8 m/s$^2$ [32.17 ft/s$^2$]).

### Image processing and analysis for pore structure characterization

Image analysis is one of the most powerful tools to characterize the pore structure of porous materials. Pore structure characterization of pervious concretes using 2D images of the material have been reported.[6,8] Pervious concrete specimens of 100 mm (4 in.) diameter and 200 mm (8 in.) length were trimmed into 150 mm (6 in.) long cylindrical specimens by removing 25 mm (1 in.) thick slices from the top and bottom. The specimens were then prepared for imaging by sectioning the 150 mm (6 in.) long specimens into 50 mm (2 in.) thick slices. For a particular pervious concrete mixture, two cylinders were used for image analysis, thus providing six sections and 12 images. Both surfaces of the cut sections were ground sufficiently to obtain flat and smooth surfaces. The solid phase of these surfaces was carefully painted white using a permanent marker to enhance contrast between the solid and pore phases. These surfaces were scanned over a clear plastic film in grayscale mode using a flatbed scanner at a resolution of 300 dpi. A few of the images were rendered unusable because of the edge effects and surface irregularities resulting from the cutting process, and these images were not used for further analysis.

The selected images were processed and analyzed using image analysis and processing software (ImageJ©, freely available at http://rsbweb.nih.gov/ij/). The scanned images were cropped and resized into circular images of 570 pixels (95 mm [3.8 in.]) in diameter, converted into binary images by a thresholding operation to separate the pore and solid phases and enhanced to remove noise. For 3D material reconstruction from 2D images, 400 x 400 pixel (66.7 x 66.7 mm [2.67 x 2.67 in.]) square images were obtained from the circular images. The pore structure features such as the area fraction of pores, pore sizes, mean free spacing (defined as the average value of uninterrupted surface-to-surface distance between all of the neighboring pores), and the specific surface area of pores (the surface area of the boundary between the pore phase and the solid) of these pervious concrete mixtures were extracted from these square images. The aforementioned characteristics of the pore phase of different pervious concrete specimens are evaluated in detail to facilitate comparisons with the pore structure features of the computationally reconstructed 3D pervious concrete specimens that will be used for permeability prediction. Detailed information on the determination of each of these pore structure features can be found in recent publications.[8,18]

To ensure that cropping a 570 pixel circular image to a 400 x 400 pixel (66.7 x 66.7 mm [2.67 x 2.67 in.]) square image does not result in appreciable changes in the measured pore structure features, the area fraction of pores in the

parent 570 pixel circular images, and the cropped 400 x 400 pixel (66.7 x 66.7 mm [2.67 x 2.67 in.]) square images were determined and are compared in Table 1 along with the volumetric porosities (the average value of measured porosities corresponding to three to four cylinders) of different mixtures. The measured porosities (volumetric or area fraction) for different pervious concrete mixtures ranged from 16 to 28% with a maximum variation of approximately 20% between the volumetric and image analysis-based methods. The area fractions of pores obtained from circular or square images are found to be similar. The average values for the circular images are consistently greater, likely indicating a wall effect[19] producing enhanced porosity near the walls of the cylinder. Table 1 also shows the number of 400 x 400 pixel (66.7 x 66.7 mm [2.67 x 2.67 in.]) square images used for the analysis. It can be seen from Table 1 that the measured volumetric porosity values ($\phi_V$) and area fraction of pores ($\phi_A$) are close for most of the pervious concrete mixtures. This is in conformance with the stereological theory that states that if random samples are used, the pore area fraction of the 2D image should be equal to the volume fraction of pores ($\phi_V$).[20]

## 3D MATERIAL STRUCTURE RECONSTRUCTION AND COMPARISON OF REAL AND RECONSTRUCTED STRUCTURES

### Reconstruction of 3D structure from 2D images

A correlation filter-based 3D reconstruction algorithm[13,17,21,22] was used to generate 3D pervious concrete structures using starting 2D images from actual specimens. As described in a previous section, 400 x 400 pixel (66.7 x 66.7 mm [2.67 x 2.67 in.]) square images were used for 3D reconstruction.

The first step in the reconstruction process is to obtain two-point correlation (TPC) functions for the pore phase of the material. The TPC function is a statistical measure of the pore structure obtained by randomly throwing line segments of length "$l$" into a two-phase material structure and counting the fraction of times both end points of the line lie in the phase of interest.[23] It contains information about the area fraction of pores, characteristic pore sizes, and the specific surface area of pores.[15,24,25] A typical TPC function for a pervious concrete mixture having 23% porosity is shown in Fig. 1. The value of the TPC function at $l = 0$, [$S_2$ ($l = 0$)], corresponds to the pore area fraction of the image ($\phi_A$), and the value of $S_2(l)$ when the function plateaus correspond to $\phi_A^2$. The intersection of the slope of $S_2(l)$ at $l = 0$ and the plateau region denotes a characteristic dimension of the pore structure ($l_{TPC}$). This characteristic dimension can be used to define the average pore diameter ($d_{TPC}$) as[11]

$$d_{TPC} = l_{TPC}/(1 - \phi_A) \quad (1)$$

The slope of $S_2(l)$ at $l = 0$ can be related to the specific surface area of the pores $s_p$ (ratio of the pore surface area to the total volume of the sample) as[11]

$$\lim_{l \to 0} \frac{\partial S_2(l)}{\partial l} = -\frac{s_p}{4} \quad (2)$$

The 3D reconstruction algorithm along with the TPC function was used to reconstruct 300 x 300 x 300 voxel digitized 3D material structures having a similar volumetric porosity ($\phi_V$),

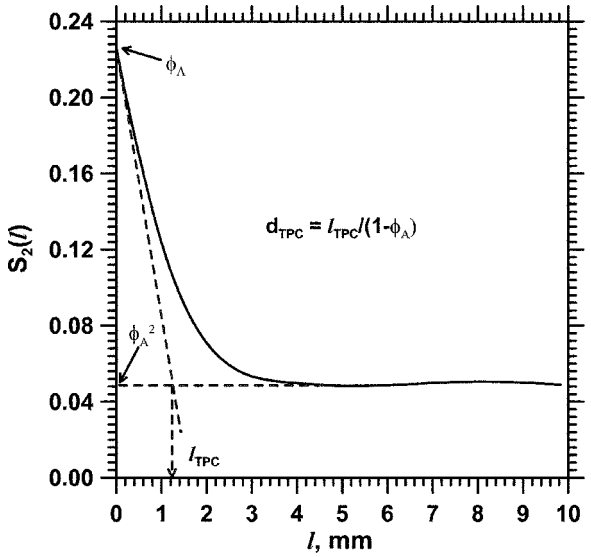


*Fig. 1—TPC function for typical pervious concrete mixture ($\phi_A$ is pore area fraction of image; $l_{TPC}$ is characteristic dimension of pore structure; and $d_{TPC}$ is average pore diameter). (Note: 1 mm = 0.0394 in.)*

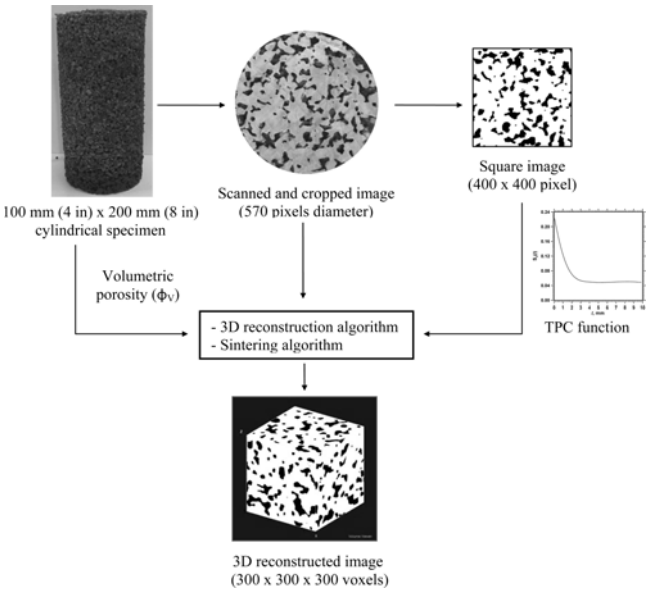


*Fig. 2—Schematic of 3D reconstruction process.*

pore surface area, and correlation function as that of the real pervious concrete specimens. The hydraulic radii (ratio of the cross-sectional area of the pore to its perimeter, or the ratio of total pore volume to the total surface area of pores) of these reconstructed structures were found to be lower than those of the original 2D images used for reconstruction. Hence, a sintering algorithm[13] was used to modify the reconstructed structures to bring their hydraulic radii closer to that of the parent image. Figure 2 shows a schematic of the steps involved in the 3D reconstruction process. The computer programs used for the reconstruction can be accessed at ftp://ftp.nist.gov/pub/bfrl/bentz/permsolver.

For a particular pervious concrete mixture, the 400 x 400 pixel (66.7 x 66.7 mm [2.67 x 2.67 in.]) 2D images (the number of such images available are given in Table 1, although only four or five of them were used to reconstruct 3D structures),

**Table 1—Porosities of pervious concrete mixtures used in this study determined using volumetric and image analysis-based methods**

| No. | Mixture ID | Volumetric porosity $\phi_V$, % | | Area fraction of pores $\phi_A$, % | | | | |
|---|---|---|---|---|---|---|---|---|
| | | | | Circular images (570 pixels) | | Square images (400 x 400 pixels) | | |
| | | Average value* | Standard deviation* | Average value | Standard deviation | No. of images | Average value | Standard deviation |
| 1 | 100 – #8 | 19.9 | 2.0 | 21.7 | 4.4 | 7 | 20.2 | 3.9 |
| 2 | 100 – #4 | 19.4 | 1.2 | 20.2 | 4.0 | 5 | 19.4 | 5.2 |
| 3 | 100 – 3/8” | 19.9 | 0.7 | 17.8 | 1.7 | 7 | 15.5 | 2.8 |
| 4 | 75 – #8 – 25 – #4 | 20.9 | 0.5 | 24.6 | 3.7 | 7 | 23.1 | 3.3 |
| 5 | 50 – #8 – 50 – #4 | 21.6 | 3.9 | 22.8 | 1.8 | 8 | 21.6 | 2.1 |
| 6 | 25 – #8 – 75 – #4 | 23.7 | 2.2 | 23.0 | 2.7 | 12 | 22.3 | 2.9 |
| 7 | 75 – #8 - 25 – 3/8” | 24.9 | 0.5 | 27.9 | 1.0 | 4 | 26.2 | 1.0 |
| 8 | 50 – #8 - 50 – 3/8” | 20.6 | 0.7 | 24.7 | 2.0 | 5 | 23.4 | 1.9 |
| 9 | 25 – #8 - 75 – 3/8” | 25.1 | 1.2 | 25.4 | 2.7 | 5 | 22.6 | 1.6 |
| 10 | 75 – #4 - 25 – 3/8” | 22.0 | 2.1 | 22.0 | 3.0 | 8 | 21.0 | 3.0 |
| 11 | 50 – #4 - 50 – 3/8” | 20.6 | 3.9 | 22.6 | 3.1 | 10 | 22.6 | 2.7 |
| 12 | 25 – #4 - 75 – 3/8” | 18.7 | 1.6 | 17.6 | 3.0 | 4 | 17.1 | 2.6 |

*Average and standard deviation of porosities from three to four pervious concrete cylinders corresponding to particular mixture.

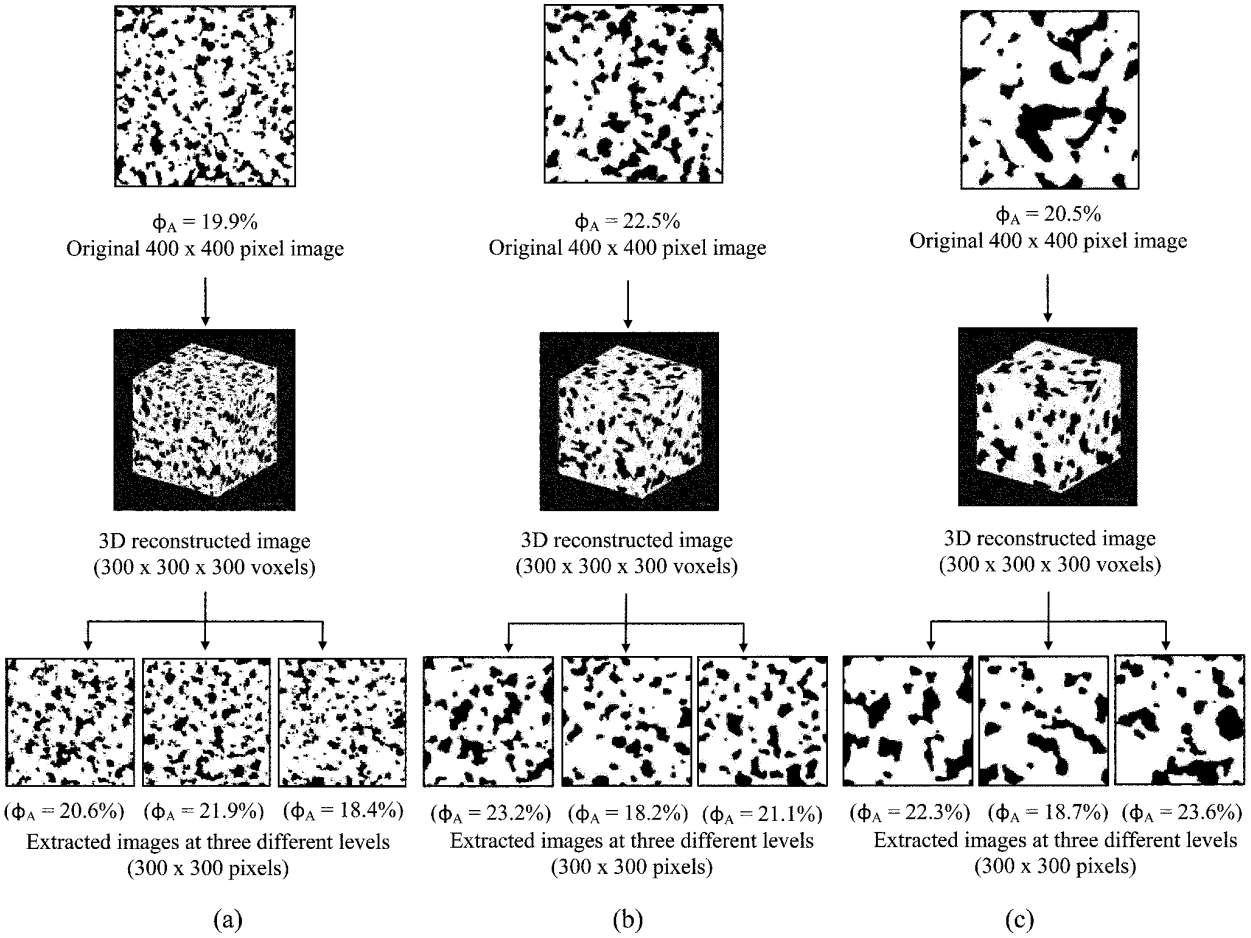


*Fig. 3—Original 2D images, reconstructed 3D material structures, and extracted 2D images from reconstructed 3D material structure for pervious concretes made with: (a) 100% No. 8; (b) 100% No. 4; and (c) 100% 3/8 in. (9.5 mm) aggregates.*

along with their TPC functions, were used to construct separate 3D structures of the material. A comparison of the normalized TPC functions

$$\left[\frac{S_2(l) - S_2(0) \times S_2(0)}{S_2(0) - S_2(0) \times S_2(0)}\right]$$

for eight to 10 2D images of the different pervious concrete mixtures were carried out. Whereas the normalized TPC functions of the different images corresponding to a particular mixture were found to be generally similar, the variability in normalized TPC functions for different images of the blended aggregate mixture was observed to be slightly higher. This could be interpreted as being contributed by the greater heterogeneity in the material.

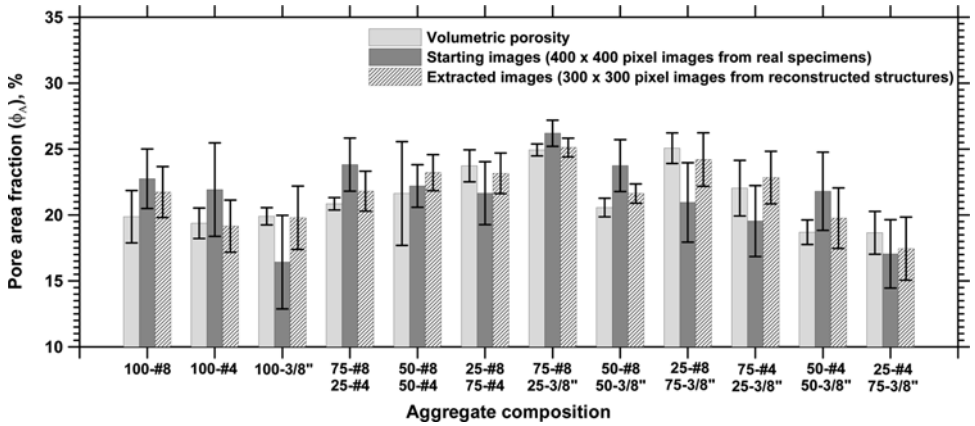


*Fig. 4—Comparison between volumetric porosities, porosities of starting 2D images, and porosities of extracted 2D images for different pervious concrete mixtures. Error bars indicate ± one standard deviation from the mean porosities. Details can be found in the text.*

Figure 3 shows typical starting images of single-sized aggregate mixtures (from real pervious concrete specimens), the reconstructed 3D structure from that image, and several 2D slices extracted from the 3D structure at different depths. Approximately 14 to 24 2D images (300 x 300 pixels) were extracted at randomly chosen depths from the different reconstructed 3D structures corresponding to a particular mixture composition, but only three are shown herein. It can be seen from these figures that the original and extracted images exhibit similar pore structure features. A detailed comparison of their pore area fractions and other pore structure features is addressed in the following section.

### Pore structure features of real and reconstructed structures

The pore structure features of the original 2D images (400 x 400 pixels) (66.7 x 66.7 mm [2.67 x 2.67 in.]) were used for 3D material reconstruction, and the pore structure features of the 2D images (300 x 300 pixels) extracted from those reconstructed 3D structures are analyzed in detail in this section. The intention of such an analysis is to examine how well the reconstruction process captures the characteristics of the pore space of the parent image. The pore structure features that are used to compare the original image and 2D images from the reconstructed structures are the pore area fractions, representative pore sizes, mean free spacing between the pores, and the specific surface area of the pores. For each pervious concrete mixture, the pore structure features of four starting 2D images that were used for 3D reconstruction were compared to 14 to 24 2D slices extracted from several reconstructed 3D structures.

### Comparison of pore area fractions

Figure 4 shows the comparison of the volumetric porosity ($\phi_V$), average pore area fractions ($\phi_A$) of parent 2D images, and the average $\phi_A$ values of several 2D images extracted from the reconstructed 3D structures for all of the pervious concrete mixtures used in this study. The error bars indicate one standard deviation of pore area fractions between different starting images (four) for the experimental values or between the 2D images (14 to 24) extracted from different 3D structures corresponding to the same pervious concrete mixture. It can be observed that the average pore area fractions of the extracted 2D images match the volumetric porosity and the average pore area fractions of the starting images fairly well. This observation is not surprising because the 3D reconstruction process involved matching the volumetric porosities of the parent specimen from which the starting images were obtained and the porosity of the reconstructed 3D structure. The volumetric porosities $\phi_V$ of the pervious concrete specimens were observed to be in agreement with the average pore area fractions of the starting images, as shown in Table 1.

### Comparison of representative pore sizes

Several image analysis-based methods are commonly used to characterize the sizes of the features of interest in porous materials. They include: 1) the cumulative frequency distribution function (cdf) of the feature sizes that provides an equivalent pore size, 2) TPC function, and 3) the granulometric density function.[8] The applicability of these methods to pervious concrete characterization has been previously reported.[8,18] In this study, the focus is on pore size extraction using the first two methods. Whereas the equivalent pore sizes ($d_{50}$, corresponding to 50% of the cdf) are reported in this paper because of their ease of measurement, the pore sizes obtained from the TPC functions are also reported because the TPC function is employed in the 3D reconstruction of pervious concrete from 2D images. A comparison of the pore sizes obtained from cdf ($d_{50}$) and the TPC function ($d_{TPC}$, obtained from Eq. (1)) is shown in Fig. 5. The data shown in Fig. 5 are from 2D images of real pervious concrete specimens. The excellent agreement between the two representative pore sizes indicates that either $d_{50}$ or $d_{TPC}$ can be used as the characteristic pore size in pervious concretes and could potentially be used in empirical equations to predict their permeability.

The equivalent pore sizes ($d_{50}$) of the starting images and the slices from 3D reconstructed structures are compared in Fig. 6. The error bars for the $d_{50}$ values of the starting images correspond to one standard deviation between four different starting images, whereas the error bars corresponding to the $d_{50}$ values of extracted images correspond to one standard deviation between 14 to 24 extracted images from different 3D reconstructed structures for the same mixture. For a majority of the pervious concrete mixtures, the $d_{50}$ values from starting images and the extracted 2D images show good agreement. In general, the $d_{50}$ values of the extracted images are observed to be slightly lower than those of the starting images. The relationship between $d_{TPC}$ of the starting and

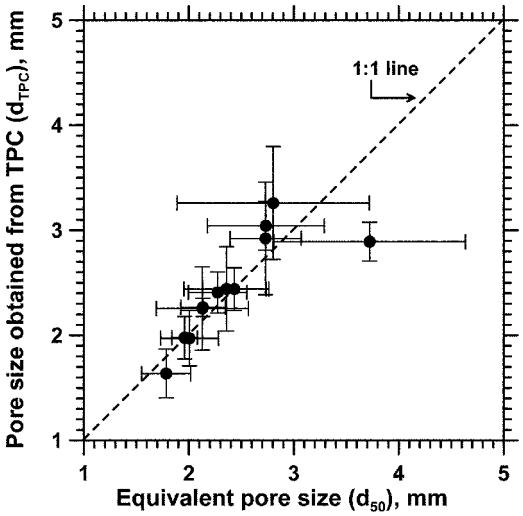


*Fig. 5—Comparison of equivalent pore sizes ($d_{50}$) and pore sizes obtained using TPC function ($d_{TPC}$). Error bars indicate ± one standard deviation from mean pore sizes. The number of images for different mixtures are given in Table 1. (Note: 1 mm = 0.0394 in.)*

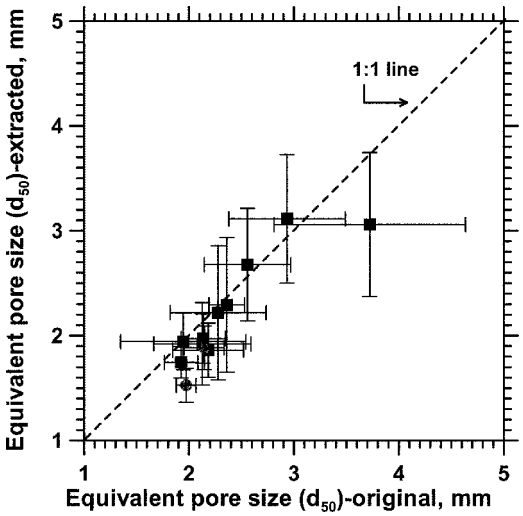


*Fig. 6: Relationship between equivalent pore sizes ($d_{50}$) obtained from original 2D images and 2D images extracted from corresponding 3D reconstructed material structures. Open circles correspond to mixtures where Mann-Whitney statistic $p < 0.05$ for $d_{50}$, as given in Table 2. Error bars indicate ± one standard deviation from mean pore sizes. (Note: 1 mm = 0.0394 in.)*

extracted images were also obtained (not shown in the paper). An excellent 1:1 relationship was observed, which is not surprising because the reconstruction process directly uses the TPC function of the original image.

## Comparison of mean free spacing and specific surface area of pores

Pore phase dispersion is generally represented using the mean free spacing parameter (λ) of pores. The value λ can be related to the pore area fraction in the image ($\phi_A$) and the perimeter length of pore features per unit area ($L_A$) as[26]

$$\lambda = \frac{\pi(1-\phi_A)\phi_A}{L_A} \quad (3)$$

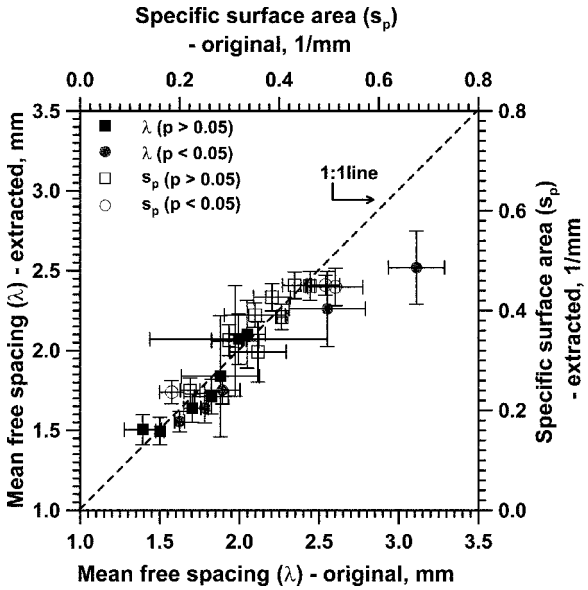


*Fig. 7—Relationship between mean free spacing (λ) and specific surface area ($s_p$) of the original 2D images and 2D images extracted from corresponding 3D reconstructed material structures. Circles correspond to mixtures where Mann-Whitney statistic $p < 0.05$ for λ and $s_p$ as given in Table 2. Error bars indicate ± one standard deviation from mean pore structure features (λ or $s_p$). (Note: 1 mm = 0.0394 in.)*

Previously, λ was observed to increase linearly with an increase in pore sizes.[8] Because the sizes of the pores in pervious concrete are proportional to the sizes of the aggregates,[8] the mean free spacing of pores can also be related to the aggregate sizes. Figure 7 shows the relationship between λ obtained from starting 400 x 400 pixel (66.7 x 66.7 mm [2.67 x 2.67 in.]) images and the average λ obtained for 14 to 24 2D images extracted from the 3D structures developed using those starting images. It can be seen that the λ values of the extracted images are in good agreement with the λ values of the original images. This shows that the reconstructed material structure retains the pore phase dispersion characteristics of the original pervious concrete specimen.

The specific surface area of the pores ($s_p$) is another important characteristic of the pore phase of a porous material. It is generally represented as the ratio of the surface area of pores to the total volume, and thus is the reciprocal of the hydraulic radius. Hydraulic radius is a convenient means to represent pores of irregular shapes; thus, $s_p$ can be used as an indicator of the pore sizes of the specimen. For monosized spherical non-overlapping pores of diameter $d$, $s_p$ has been shown to be equal to $6\phi/d$ where $\phi$ is the porosity.[15] Thus, a higher value of $s_p$ at the same pore volume indicates smaller pores. When empirical or semi-empirical relationships such as the Kozeny-Carman equation are used for the permeability prediction of porous media, $s_p$ plays a very significant role. The specific surface areas ($s_p$) of the starting images and the extracted 2D images were obtained using the measured TPC functions, as shown in Eq. (2). The $s_p$ values of the starting images and the extracted images are also compared in Fig. 7, which also shows good agreement.

**Table 2—Summary of statistical analysis of pore structure features of starting and extracted images and measured and predicted permeabilities**

| No. | Mixture ID | No. of reconstructed 3D images | No. of extracted 2D images from different 3D images | *p*-value from Mann-Whitney U-test | | | | | |
|---|---|---|---|---|---|---|---|---|---|
| | | | | Pore area fraction | $d_{50}$ | $d_{TPC}$ | λ | $s_p$ | Permeability $k$ |
| 1 | 100 – #8 | 5 | 16 | 0.103 | 0.065 | 0.156 | 0.118 | **0.037** | 0.857 |
| 2 | 100 – #4 | 4 | 24 | 0.939 | 0.768 | 0.341 | 0.776 | 0.144 | 0.533 |
| 3 | 100 – 3/8” | 4 | 22 | 0.900 | 0.546 | 0.522 | **0.001** | **0.002** | 0.133 |
| 4 | 75 – #8 – 25 – #4 | 4 | 15 | 0.248 | **0.001** | 0.986 | 0.720 | **0.010** | 0.343 |
| 5 | 50 – #8 – 50 – #4 | 4 | 15 | 0.716 | **0.030** | 0.905 | **0.020** | 0.124 | 0.267 |
| 6 | 25 – #8 – 75 – #4 | 5 | 19 | 0.655 | 0.081 | 0.626 | **0.003** | 0.081 | **0.036** |
| 7 | 75 – #8 – 25 – 3/8” | 5 | 17 | 0.633 | 0.282 | 0.753 | 0.120 | 0.317 | **0.036** |
| 8 | 50 – #8 – 50 – 3/8” | 4 | 14 | 0.053 | 0.488 | 0.265 | 0.095 | 0.086 | 0.114 |
| 9 | 25 – #8 – 75 – 3/8” | 5 | 17 | 0.427 | 0.446 | 0.574 | 0.317 | 0.052 | **0.036** |
| 10 | 75 – #4 – 25 – 3/8” | 4 | 16 | 0.784 | 0.143 | 0.617 | **0.022** | 0.335 | 0.267 |
| 11 | 50 – #4 – 50 – 3/8” | 4 | 17 | 0.226 | 0.964 | 0.893 | 0.302 | 0.857 | 0.629 |
| 12 | 25 – #4 – 75 – 3/8” | 4 | 16 | 0.392 | 0.052 | 0.422 | **0.042** | 0.138 | 0.533 |

Note: Values in bold indicate cases for which Mann-Whitney statistic is $p < 0.05$; 1 $m^2$ = 1550 $in.^2$ (10.8 $ft^2$); and 1 $m^4$ = 2.4 × $10^6$ $in.^4$ (116 $ft^4$).

### Assessing statistical similarity of pore structure features of real and reconstructed images

A detailed statistical analysis was carried out to examine the statistical similarity between the previously discussed pore structure features (pore area fractions, representative pore sizes, mean free spacing between pores, and specific surface area of the pores) of real and reconstructed structures. To assess whether the means of the pore structure features from real and reconstructed structures are similar, a parametric two-sample t-test can be used. The t-test, however, assumes a normal distribution of the values; hence, a Mann-Whitney U-test (also known as the Wilcoxon rank-sum test),[27] which is a nonparametric test that does not make any assumptions related to the distribution, was used. The Mann-Whitney U-test assesses whether the distributions of two independent samples of observations are statistically different from each other. This test is also suitable for analysis when only a smaller number of observations are available and the sample sizes are different. The null hypothesis in a Mann-Whitney U-test is that the two samples come from identical populations. A *p*-value (probability associated with the smallest level of significance that would lead one to reject the null hypothesis) greater than 0.05 indicates an acceptance of the null hypothesis at the significance level of 5% (or confidence interval of 95%). Table 2 summarizes the observed *p*-values for each pore structure feature along with the number of reconstructed 3D images and the number of 2D images extracted from different reconstructed structures. The 2D images from the real specimens and those extracted from the 3D reconstructed structures show statistical similarity for most of the pore structure features studied (where there is a statistical dissimilarity, that is, $p < 0.05$, the corresponding values are shown in bold in Table 2). For most of the pervious concrete specimens, the pore area fractions and the representative pore sizes between the real and reconstructed images are statistically similar, whereas statistical dissimilarity is slightly more prevalent for the pore structure features such as mean free spacing and specific surface area. This is not surprising because the latter two parameters are more related to the distribution of pores and thus to the heterogeneity in the material structure than the area fraction or sizes of pores. The *p*-values lower than 0.05 for certain pore structure features in some of the specimens can also be attributed to the very low variances in the values of that particular feature in the starting images, which effectively make the variances in the reconstructed structure look extremely large, and thus come to the conclusion that they are statistically dissimilar. The analysis of a larger number of starting images could minimize this effect.

## PERMEABILITY PREDICTION AND COMPARISON WITH EXPERIMENTAL VALUES

A 3D Stokes permeability solver for porous media[13,16,28-30] was used to predict the permeability of reconstructed 3D structures of pervious concretes. This solver has been recently used to predict the permeability of virtual pervious concretes.[17] To compute the permeability in one of the three principal directions (X, Y, or Z) of the reconstructed structure, a pressure gradient of one unit per voxel is applied along that particular direction. The fluid velocity vector is then calculated for slow, incompressible steady-state flow by numerically solving the linear Stokes equations using a finite difference scheme in conjunction with an artificial compressibility relaxation algorithm. Once the finite different solution converges sufficiently, the intrinsic permeability ($k$) is calculated by volume-averaging the local fluid velocity and applying the Darcy equation

$$u = -\frac{k}{\eta}\frac{\Delta P}{L} \tag{4}$$

where $u$ is the average fluid velocity in the direction of flow, $\Delta P$ is the pressure difference, $L$ is the length of the material structure where the pressure gradient was applied, and η is the fluid viscosity. For the 3D reconstructed pervious concrete structures, the permeabilities in the three principal directions were obtained by changing the direction of fluid flow. The average of the permeability values corresponding to these three directions was taken as the predicted permeability value for that 3D structure. The permeabilities were predicted for each reconstructed structure (reconstructed using different starting images of a particular mixture), and the average value was reported as the predicted permeability.

Figure 8 shows the experimental and predicted permeability values for different pervious concrete mixtures. The error bars for the experimental values show one standard deviation for the permeabilities for different pervious concrete specimens belonging to the same mixture, and the error bars for the

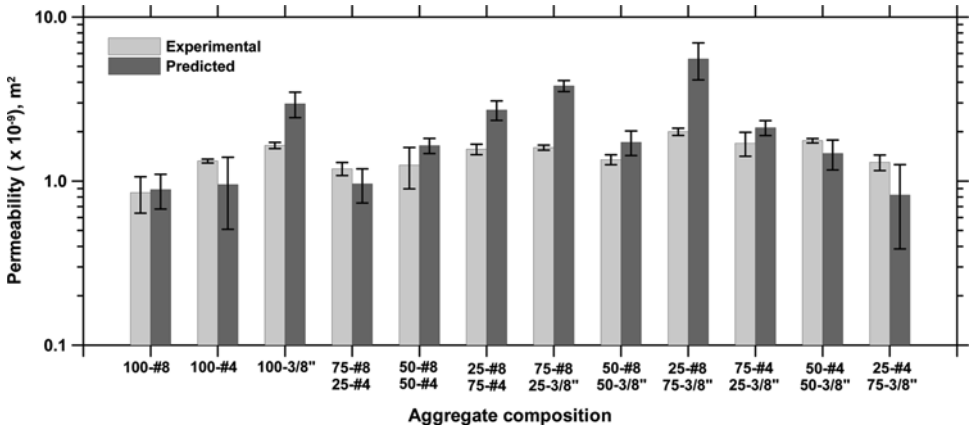


*Fig. 8—Experimental and predicted permeabilities for different pervious concrete mixtures. Error bars indicate ± one standard deviation from mean permeabilities. Details can be found in the text. (Note: 1 $m^2$ = 1550 $in.^2$)*

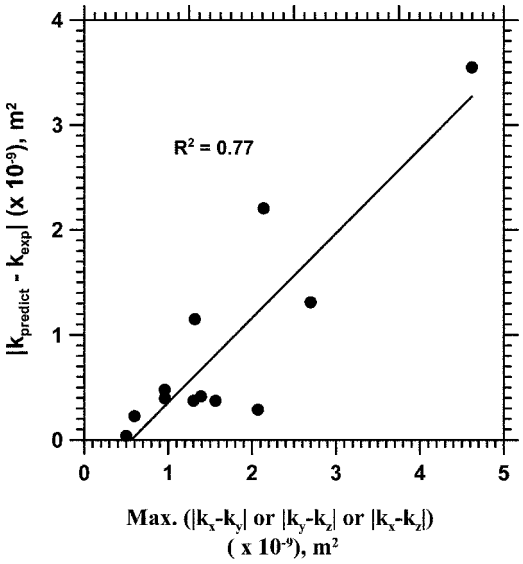


*Fig. 9—Relationship between differences between predicted and experimentally measured permeability values and maximum range of predicted permeabilities in three different directions. (Note: 1 $m^2$ = 1550 $in.^2$)*

predicted values show one standard deviation for the predicted permeabilities for different 3D structures reconstructed using different starting images corresponding to a particular mixture. It can be observed that the predicted permeability values are generally in reasonable agreement with the experimentally determined permeability values for most of the pervious concrete mixtures.

To evaluate the statistical similarity between the experimentally determined and predicted permeability values, a detailed statistical analysis was carried out. The Mann-Whitney U-test, which was described previously, was also used in this case. A *p*-value greater than 0.05 is an indication of the statistical similarity between the experimental permeability measurements and the permeability predicted from reconstructed 3D images. Table 2 shows the *p*-values from the Mann-Whitney U-test. It can be seen from this table that the *p*-values are greater than 0.05 for most of the pervious concrete mixtures except for three mixtures that have larger differences in the experimental and predicted permeability values (shown in bold in Table 2), indicating that the experimentally measured and predicted permeabilities are statistically similar for most of the cases.

The differences in the experimental and predicted permeability values observed for some of the pervious concrete mixtures in Fig. 9 could also be attributed to the assumption of homogeneity and isotropy made in the 3D reconstruction process. It needs to be remembered that pervious concrete is not a homogeneous and isotropic material, and the degree of homogeneity varies with the material design parameters such as the aggregate size. The distribution of pores could be less homogeneous for specimens made with larger-sized aggregates, as can be seen from Fig. 3(c). Also, in some blended aggregate mixtures, the interaction effect between the dominant and less dominant particle sizes result in either a loosening effect (particles spaced further apart) or local pore filling effect (some smaller particles filling in the voids between the larger particles), which could result in less than satisfactory adherence to the assumptions of representative elementary volume, homogeneity, and isotropy. To quantitatively examine this effect, the maximum differences between the predicted permeabilities in each of the X, Y, and Z directions, max($|k_x-k_y|$, $|k_x-k_z|$, $|k_y-k_z|$) from the reconstructed material structures are plotted against the absolute difference between the predicted ($k_{predict}$) and experimentally measured ($k_{exp}$) permeabilities in Fig. 9. A larger difference between the experimental and predicted permeability values is seen to be linked to this maximum. Large differences between $k_x$, $k_y$, and $k_z$ are indications of the anisotropy of the reconstructed material, which may indicate a finite size effect.

## CONCLUSIONS

This paper has dealt with 3D reconstruction of pervious concrete structures from starting 2D images of 12 different pervious concrete mixtures, using the reconstructed structures to predict their permeability. TPC functions were extracted from the starting 2D images, which were used along with the measured volumetric porosity and a sintering algorithm to reconstruct 3D structures. The pore structure features such as pore area fractions, representative pore sizes, mean free spacing between the pores, and the specific surface area of the pores of the starting images and 2D slices from the reconstructed 3D structures were compared. The pore structure features of the 2D slices from reconstructed 3D structures were found to be in generally good agreement with those of starting 2D images, showing that the reconstructed 3D

material structure retains the characteristics of the pore structure of the parent material, facilitating reasonably accurate predictions of the material performance. A statistical analysis using a nonparametric test (Mann-Whitney U-test) was also carried out to establish the similarity between the real and reconstructed material structures.

A Stokes permeability solver was used on the 3D reconstructed structures to predict the permeability. The experimentally measured and the predicted permeabilities showed good agreement for most of the pervious concrete mixtures. Mann-Whitney U-tests were also carried out to ascertain the similarity between the experimentally determined and predicted permeability values. The possibility of violation of the assumptions of a representative elementary volume, homogeneity, and isotropy in the 2D and 3D material structures was evaluated using the maximum range in the predicted permeabilities in the X, Y, and Z directions and the absolute difference between the experimental and predicted permeabilities; a larger maximum range was found to correspond to a greater difference between experiment and prediction. The reconstructed material structures could also find future use in providing indicators of the changes in: 1) the transport performance of the material during service such as pore constriction and connectivity reduction due to particle trapping (clogging), or 2) 3D pore space as a result of changes in mixture proportions.

## ACKNOWLEDGMENTS

The third author gratefully acknowledges funding from a CAREER award (CMMI 0747897) from the National Science Foundation (NSF) in support of this work. The authors also extend their appreciation to O. Deo, a graduate student at Clarkson, for his help with specimen preparation.

## REFERENCES

1. ACI Committee 522, "Pervious Concrete (ACI 522R-06)," American Concrete Institute, Farmington Hills, MI, 2006, 25 pp.

2. Neithalath, N., "Development and Characterization of Acoustically Efficient Cementitious Materials," PhD thesis, Purdue University, West Lafayette, IN, 2004, 269 pp.

3. Neithalath, N.; Marolf, A.; Weiss, J.; and Olek, J., "Modeling the Influence of Pore Structure on the Acoustic Absorption of Enhanced Porosity Concrete," *Journal of Advanced Concrete Technology*, V. 3, No. 1, Feb. 2005, pp. 29-40.

4. Neithalath, N; Weiss, J.; and Olek, J., "Characterizing Enhanced Porosity Concrete Using Electrical Impedance to Predict Acoustic and Hydraulic Performance," *Cement and Concrete Research*, V. 36, 2006, pp. 2074-2085.

5. Meininger, R. C., "No-Fines Pervious Concrete for Paving," *Concrete International*, V. 10, No. 8, Aug. 1988, pp. 20-27.

6. Low, K.; Harz, D.; and Neithalath, N., "Statistical Characterization of the Pore Structure of Enhanced Porosity Concrete," *Proceedings of the 2008 Concrete Technology Forum*, National Ready Mix Concrete Association, Denver, CO, 2008. (CD-ROM)

7. Tennis, P. D.; Leming, M. L.; and Akers, D. J., "Pervious Concrete Pavements," Portland Cement Association, Skokie, IL, 2004, 28 pp.

8. Sumanasooriya, M. S., and Neithalath, N., "Stereology and Morphology-Based Pore Structure Descriptors of Enhanced Porosity (Pervious) Concretes," *ACI Materials Journal*, V. 106, No. 5, Sept.-Oct. 2009, pp. 429-438.

9. Marolf, A.; Neithalath, N.; Sell, E.; Wegner, K.; Weiss, J.; and Olek, J., "Influence of Aggregate Size and Gradation on Acoustic Absorption of Enhanced Porosity Concrete," *ACI Materials Journal*, V. 101, No. 1, Jan.-Feb. 2004, pp. 82-91.

10. Montes, F., and Haselbach, L., "Measuring Hydraulic Conductivity in Pervious Concrete," *Environmental Engineering Science,* V. 23, No. 6, 2006, pp. 956-965.

11. Berryman, J. G., and Blair, S. C., "Kozeny-Carman Relations and Image Processing Methods for Estimating Darcy's Constant," *Journal of Applied Physics*, V. 62, Sept. 1987, pp. 2221-2228.

12. Katz, A. J., and Thompson, A. H., "Quantitative Prediction of Permeability in Porous Rock," *Physical Review B*, V. 34, No. 11, 1986, pp. 8179-8181.

13. Bentz, D. P., and Martys, N. S., "Hydraulic Radius and Transport in Reconstructed Model Three-Dimensional Porous Media," *Transport in Porous Media*, V. 17, No. 3, 1994, pp. 221-238.

14. Bentz, D. P., "CEMHYD3D: A Three-Dimensional Cement Hydration and Microstructure Development Modeling Package," *Report* 7232, Version 3.0, National Institute of Standards and Technology Interagency, Technology Administration, U.S. Department of Commerce, June 2005.

15. Garboczi, E. J.; Bentz, D. P.; and Martys, N. S., "Digital Images and Computer Modeling," *Experimental Methods in the Physical Science, Methods in the Physics of Porous Media*, V. 35, 1999, pp. 1-41.

16. Bentz, D. P., and Martys, N. S., "A Stokes Permeability Solver for Three-Dimensional Porous Media," NISTIR 7416, U.S. Department of Commerce, 2007, 227 pp.

17. Bentz, D. P, "Virtual Pervious Concrete: Microstructure, Percolation, and Permeability," *ACI Materials Journal*, V. 105, No. 3, May-June 2008, pp. 297-301.

18. Neithalath, N.; Bentz, D. P.; and Sumanasooriya, M. S., "Advances in Pore Structure Characterization and Performance Prediction of Pervious Concretes," *Concrete International*, V. 32, No. 5, May 2010, pp. 35-40.

19. de Larrard, F., *Concrete Mixture Proportioning: A Scientific Approach*, E&FN Spon, London, UK, 1999, 448 pp.

20. Hu, J., and Stroeven, P., "Proper Characterization of Pore Size Distribution in Cementitious Materials," *Key Engineering Materials*, V. 302-303, 2006, pp. 479-485.

21. Joshi, M., "A Class of Stochastic Models for Porous Media," PhD thesis, University of Kansas, Lawrence, KS, 1974, 163 pp.

22. Quiblier, J. A., "A New Three-Dimensional Modeling Technique for Studying Porous Media," *Journal of Colloid and Interface Science*, V. 98, No. 1, 1984, pp. 84-102.

23. Torquato, S., *Random Heterogeneous Materials—Microstructure and Macroscopic Properties*, Springer Science and Business Media LLC, 2002, 728 pp.

24. Berryman, J. G., "Measurement of Spatial Correlation Functions Using Image Processing Techniques," *Journal of Applied Physics*, V. 57, Apr. 1985, pp. 2374-2384.

25. Berryman, J. G., and Blair, S. C., "Use of Digital Image Analysis to Estimate Fluid Permeability of Porous Materials: Application of Two-Point Correlation Functions," *Journal of Applied Physics*, V. 60, Sept. 1986, pp. 1930-1938.

26. Hu, J., "Porosity of Concrete. Morphological Study of Model Concrete," PhD thesis, Delft University, the Netherlands, 2004, 159 pp.

27. Bernstein, S.; and Bernstein, R., "Elements of Statistics II: Inferential Statistics," *Schaum's Outline Series*, McGraw Hill, 2000, 350 pp.

28. Schwartz, L. M.; Martys, N.; Bentz, D. P.; Garboczi, E. J.; and Torquato, S., "Cross-Property Relations and Permeability Estimation in Model Porous Media," *Physical Review E*, V. 48, No. 6, 1993, pp. 4584-4591.

29. Martys, N., and Garboczi, E. J., "Length Scales Relating the Fluid Permeability and Electrical Conductivity in Random Two-Dimensional Model Porous Media," *Physical Review B*, V. 46, 1992, pp. 6080-6095.

30. Martys, N. S.; Torquato, S.; and Bentz, D. P., "Universal Scaling of Fluid Permeability for Sphere Packing," *Physical Review E*, V. 50, No. 1, 1994, pp. 403-408.